

Gamma-ray modulation properties of tungsten coded apertures for a novel mixed-field imaging system

Michal J. Cieslak^{*1}, Kelum A.A. Gamage², Robert Glover³, and C. James Taylor⁴

^{1,4}*Department of Engineering, Lancaster University, Lancaster LA1 4YW, UK*

²*School of Engineering, University of Glasgow, Glasgow G12 8QQ, UK*

³*Radiometric Systems Group, Sellafield Ltd, Seascale CA20 1PG, UK*

28th January 2019

Abstract

An investigation into the gamma-ray modulation properties of a tungsten coded aperture, whose design is based on the mathematical principles of Modified Uniformly Redundant Arrays (MURA), has been performed. Due to the small size of the individual cells, the aperture was built using additive manufacturing methods. The gamma-ray field was produced by a ^{137}Cs radioactive isotope at Lancaster University, UK. An organic plastic scintillator sample, which is capable of pulse shape discrimination, has been used to detect the gamma-ray field modulated by a tungsten aperture. Prior to the investigation of the aperture modulation properties, energy calibration of the scintillator was performed. Its pulse shape discrimination capabilities were verified using a ^{252}Cf fission source. In this study, each of 169 coded aperture cells was investigated by collimating the modulated gamma-ray field of ^{137}Cs through a 25.4 mm thick lead supporting plate. The supporting plate has one opening in the centre, of the same dimensions as the single aperture cell, i.e. 2.5 mm \times 2.5 mm. The number of pulses detected for every aperture location were recorded in an array. The array was subsequently used to create a two-dimensional image of the source, which was encoded through the coded aperture pattern. Finally, the image was decoded using deconvolution techniques to reveal the actual source location. The new results obtained in this study indicate that sufficient gamma-ray modulation properties of the aperture can be determined, despite the relatively small footprint and thickness of the coded aperture.

1 Introduction

Coded-aperture imaging is a well-established and widely applied concept of optics, and is frequently incorporated into a range of other research fields [1]. Radiation detection is one of the examples, where there is a particular focus on X-ray and gamma-ray imaging systems [2, 3]. In recent years, however, coded-aperture based neutron imaging has seen considerably increased attention [4, 5]. A detailed account of coded-aperture based systems for radiation detection, including discussion of design and implementation methods, has been previously presented [6].

The main advantage of coded-aperture imaging is the increased signal-to-noise-ratio (SNR), when compared to single opening pinhole devices. In the latter case, there is always a trade-off between the resolution and SNR. An ideal pinhole device would require an infinitely small opening in the aperture, to achieve the highest resolution. At the same time, the opening would need to be infinitely large to obtain the highest SNR. Development of scatter-hole, and later coded-aperture techniques offer a form of a compromise between SNR and resolution [7, 8]. Due to multiple small sized openings of the aperture, it has become possible to increase the overall opening percentage of the aperture to approximately 50%.

Studies of neutron imaging systems based on coded masks that utilise organic scintillators as sensitive detectors are primarily designed as large scale detectors. For instance, Griffith et al. [4] use $15 \times 15 \times 10 \text{ cm}^3$ blocks of high-density polyethylene as single cells of a 144 element coded aperture. The detector

^{*}m.cieslak@lancaster.ac.uk

array in the study comprises of 64 cubic liquid scintillation detectors (EJ-309) of $15 \times 15 \times 10 \text{ cm}^3$ each. Another study conducted by Newby et al. [9] reports a system where a single block of the detector has dimensions $13.5 \times 13.5 \times 50 \text{ mm}^3$. In this case, the single blocks are combined into 8×8 arrays. These are further combined into a 3×3 array to build a $33.7 \times 33.7 \text{ cm}^2$ detector.

Such devices are neither easily portable nor easily deployable in the field. Therefore, they are not suitable for nuclear decommissioning applications, where the detectors are often required to survey small enclosed areas. These areas are often difficult to access by people, let alone by large machinery. Hence, the present article considers a small scale coded aperture, for which the single opening dimensions are $2.8 \times 2.8 \times 25 \text{ mm}^3$. When complemented by a suitably sized sensitive organic detector, such a system could be packaged into a portable device for nuclear decommissioning applications.

1.1 Design considerations

Depending on the application of a coded aperture in a system, a number of key features of the aperture require careful consideration at the design stage. Thickness and material type define the stopping power of the coded aperture. The aperture is expected to block the incoming particles on its opaque elements. Hence, the distance that a particle can travel in a specific material before an interaction occurs necessitates close investigation. High density chemical elements, such as lead and tungsten, are known for their good gamma-ray stopping capabilities, whereas neutron stopping properties are more complex (defined by cross-sections for specific energy ranges) and closely related to neutron's kinetic energy. Isotopes such as ^{10}B , ^7Li , ^{113}Cd and ^{157}Gd exhibit large thermal neutron cross-sections, while ^1H shows a greater fast neutron cross-section.

Therefore, for the requirements of an empirical study, a material capable of blocking both neutrons and gamma-ray photons was sought. Our earlier Monte-Carlo simulation study revealed that a W- ^{113}Cd composition (75%-25% ratio) provides optimal results [10]. However, due to safety concerns related to the handling of ^{113}Cd , a pure tungsten coded aperture was built for the present study and only tested in relation to gamma-ray modulation properties. The model drawing used for simulation and the manufactured tungsten coded apertures for the experimental work are presented in Fig. 1a and 1b, respectively.

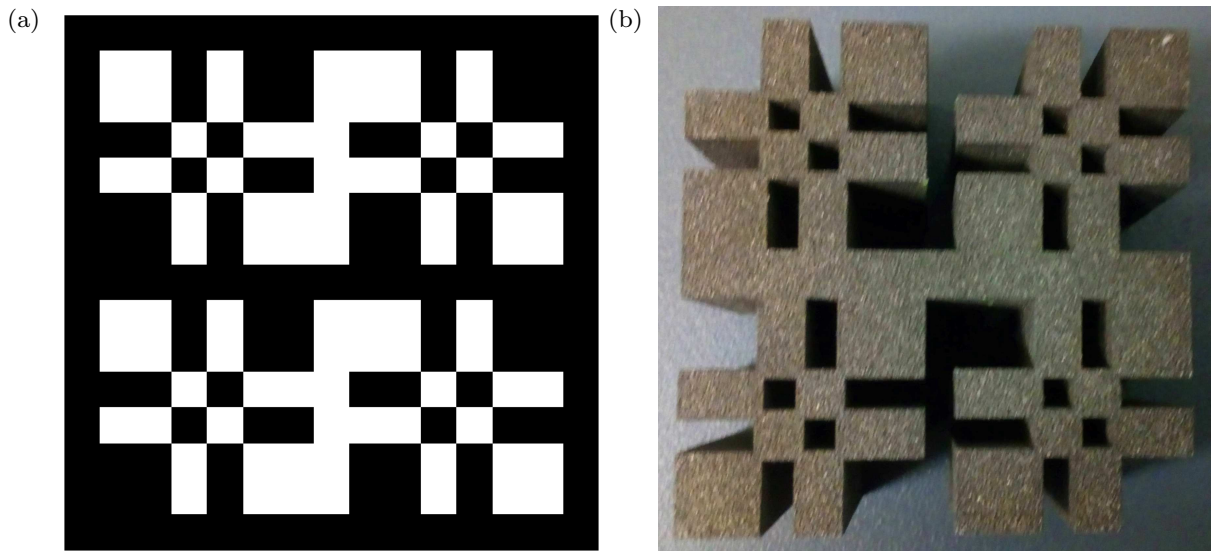


Figure 1: Coded-aperture designed for the requirements of this study, including a) initial simulated design with a transparent cell size of $2.8 \times 2.8 \times 25 \text{ mm}^3$ and b) manufactured in tungsten by M&I Materials Ltd. with a transparent cell size reduced to $2.5 \times 2.5 \times 25.4 \text{ mm}^3$, due to the fragility of the link to a single opaque element of the aperture.

Another key feature that needs to be carefully considered is the pattern of the array to be used as the coded aperture. The most extensively used patterns are Uniformly Redundant Arrays (URAs) and Modified Uniformly Redundant Arrays (MURAs) [8, 11]. In both cases, the rank of the aperture defines

the number of pixels in the particular pattern. For instance, the rank-7 aperture utilised in the present study comprises 169 cells (arranged into a 13×13 array). For an extensive review of array patterns as applied to coded apertures, as well as their design rules and associated mathematical calculations, the reader is referred to the authors' previous work [6].

Generally, the higher the rank of the aperture, the higher the resolution of the reconstructed image. However, as the rank of the aperture becomes higher, the associated pixel size decreases. As a result, the sensitive detector and accompanying photodetector would have to be of very small dimensions to provide the required one-to-one interface. Therefore, in this work, a rank-7 MURA based coded-aperture with a $2.8 \times 2.8 \times 25.4 \text{ mm}^3$ cell size was built. In this manner, it will be feasible to match the cell with a similarly sized sensitive detector and photodetector in the future.

1.2 Sensitive detectors

Regardless of the application, coded-aperture imaging requires a sensitive detector, whose task is to detect the image that is modulated through the transparent and opaque elements of the aperture. The detector's efficacy with regard to the identification of specific particle types is vital for the accurate acquisition of the modulated "image". This is subsequently used for the reconstruction of an actual image, in line with conventional image reconstruction techniques [6]. A requirement of the present study is that the detector provides good energy resolution, as well as pulse shape discrimination (PSD) potential. Therefore, a PSD capable organic plastic scintillator sample was chosen for the experiments.

Hence, the research contributions of this article relate to an experimental study of the gamma-ray modulation properties of a tungsten coded-aperture using a PSD capable sensitive detector. The key novelty is the relatively small footprint and thickness of the coded aperture. To the authors knowledge, this represents the first time that a tungsten coded aperture of this scale has been tested with regard to its gamma-ray modulation capabilities. The following section 2 describes the methodology. The results and discussion are presented in sections 3 and 4 respectively, followed by the conclusions in section 5, where potential future improvements to the system are also presented.

2 Methodology

The present section considers methods for detector calibration, PSD and the modulation capabilities of the coded aperture.

2.1 Detector calibration

Before the assessment of the modulation properties of tungsten coded aperture commenced, it was required to conduct energy calibration of the scintillation detector. The scintillator used in this study was an organic plastic PSD sample (25mm diameter, 25mm thick) provided by Lawrence Livermore National Laboratory (LLNL), U.S.A. - denoted by the LLNL number 5706. The sample was previously compared to two other solid organic scintillators in regard to its neutron/gamma discrimination properties [12]. However, no information about its energy calibration was presented in the referenced work.

In this study, the back and side of the scintillator sample was covered with EJ-510 reflective coating. The sample was subsequently coupled to an ET Enterprises 9107B photomultiplier tube (PMT) with EJ-550 silicone grease. A light-proof enclosure was placed around the scintillator-PMT assembly. The PMT was connected to a positive high voltage power supply of 860 V. Finally, an FPGA based 12-bit resolution, 500 MS/s "raw data" digitising system was used to collect the detected pulses. It collected 128 samples (every 2 ns) for every triggered pulse, with peak usually occurring between sample 50 and 70. Average rise time of a signal was estimated to 14 ns.

The assembly was exposed in turn to ^{137}Cs and ^{22}Na gamma-ray sources of 319 kBq and 1.68 kBq current activity, respectively. The sources were placed 15 cm away from the front of the detector while measurements were being taken. Given the respective activities of the sources, 120,950 ^{137}Cs pulses and 36,548 ^{22}Na pulses were accepted. Each detected pulse was digitally verified against pile-up by a custom rejection algorithm. Here, a pulse was rejected if there were two peaks detected within the same triggered window.

Recorded pulse height spectra were plotted for both gamma-ray emitters to compute the corresponding Compton edges. Pulse height spectra are presented in Fig. 2a. These were subsequently used to convert the pulse height values to electron equivalent energy for both calibration sources. ^{137}Cs produces a Compton edge of 477 keV, and ^{22}Na produces two Compton edges of 341 keV and 1062 keV gamma-ray interactions. A linear relationship between the pulse height values and corresponding electron equivalent energy is assumed, as shown in Fig. 2b. However, ^{22}Na energy spectrum in Fig. 2a, where 1062 keV Compton edge appears unusually pronounced, suggests a non-linear response of the detector. Moreover, the discrepancies between the linear fit and the estimated Compton edges on the graph in Fig. 2b further support the claim of the non-linear response of the detector. Poisson approximation of the distribution was assumed to determine the corresponding uncertainty, which is also marked on the graph in Fig. 2b for the estimated pulse height.

2.2 Pulse shape discrimination performance of the detector

Pulse shape discrimination performance of the plastic scintillator sample was previously investigated in comparison to other organic scintillator samples [12]. However, a relatively low sampling rate digitiser was utilised and the low energy limit was not investigated. In the present work, the charge comparison method (CCM) was used to perform PSD, and the low energy discrimination limit (in terms of electron equivalent energy) was sought [13]. The discrimination factor D_f was calculated using Eq. 1, in which I_{long} denotes the integral calculated over the entire tail of the pulse, with the peak of the pulse represented by the first sample, and I_{short} is calculated as an integral between the first sample being taken 32 ns after the peak and the last sample of the entire window. The way CCM was realised on the signal is exemplified in Fig. 3.

$$D_f = 1 - \frac{I_{short}}{I_{long}} \quad (1)$$

A mixed field environment was provided by the ^{252}Cf source located at Lancaster University, UK. The aforementioned assembly comprising the PMT and the organic plastic scintillator sample was exposed to the ^{252}Cf radioactive isotope. The source is normally stored in the centre of a water tank and is pneumatically moved to the edge of the tank, when required to be exposed for taking measurements. The detector assembly was placed 15 cm away from the edge of the tank, where the source is located when in exposed position. Very good pulse separation can be observed for the chosen sample, with an illustrative PSD scatter plot shown in Fig. 4. Here, the upper plume depicts the gamma-ray photon interactions and the lower plume the neutron interactions. The curved shape of the plumes reflects the aforementioned non-linear response of the detector. Nonetheless, detector's non-linear response has no significant effect on the performance of the system presented in the following sections.

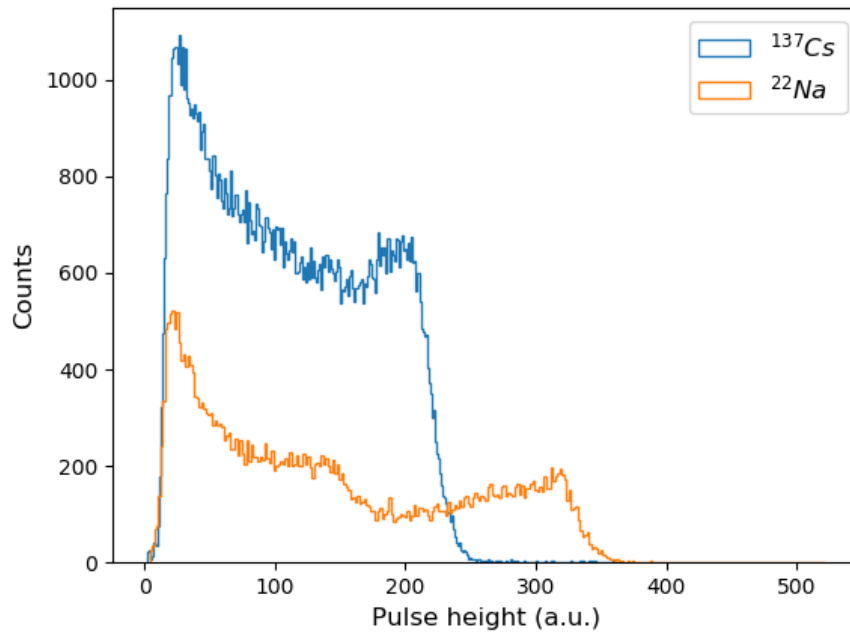
2.3 Modulation capabilities of tungsten coded aperture

Before the coded aperture was manufactured, the part was first designed in Computer-Aided Design (CAD) software and subsequently translated into Monte-Carlo code for simulation. Following completion of the simulation study, the model was built into a part using additive manufacturing techniques by M&I Materials Ltd, Manchester, UK.

Due to the complexity and small dimensions of the coded aperture, the design used for simulation work (shown in Fig. 1a), with each cell of $2.8 \times 2.8 \times 25.4 \text{ mm}^3$, was revised somewhat (Fig. 1b). This is due to the fragility of the links between single opaque cells and other parts of the coded aperture. As a result, the single transparent cell of the coded aperture was reduced to $2.5 \times 2.5 \times 25.4 \text{ mm}^3$, so that the thickness of the link to a single opaque element of the aperture could be at least 0.8 mm.

The experimental setup is presented in Fig. 5a. The green holder is used to place the plastic disk with the radioactive source. The tungsten coded aperture is placed 10 cm below the radioactive source holder – directly on top of the supporting lead plate. The CAD image of the lead supporting plate, the purpose of which was to collimate the gamma-ray photons on to the front of the detector, is shown in Fig. 5b. The front of the detector assembly is placed directly underneath the bottom of the lead supporting plate. The total distance between the bottom of the source holder and the top of the detector assembly is 15 cm.

(a)



(b)

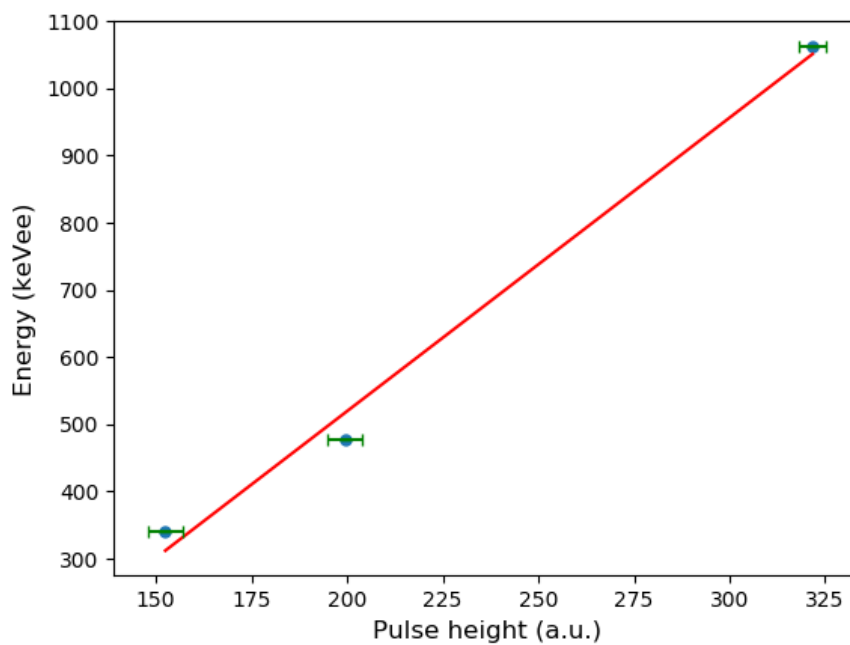


Figure 2: Energy calibration performed with ^{137}Cs and ^{22}Na showing a) pulse height spectra and b) the relationship between the pulse height and electron equivalent energy.

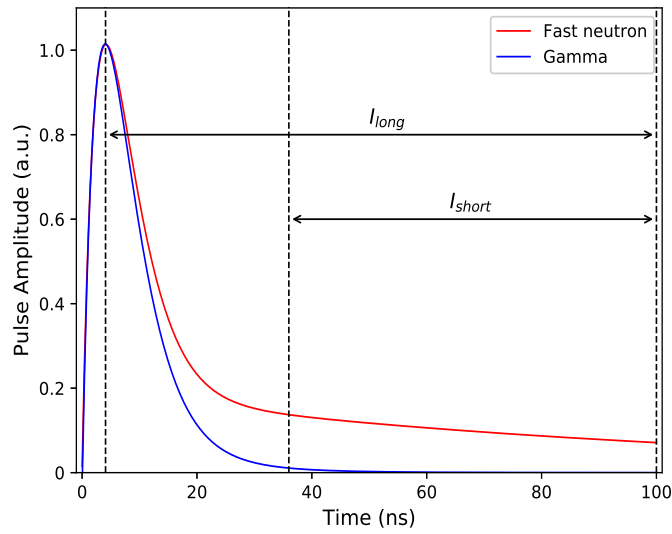


Figure 3: Theoretical fast neutron and gamma-ray scintillation pulses induced in an organic solid scintillation medium based on the information from Knoll [14] and Zaitseva et al. [15]. The way CCM was realised is presented, with the long and short integrals marked on the plot.

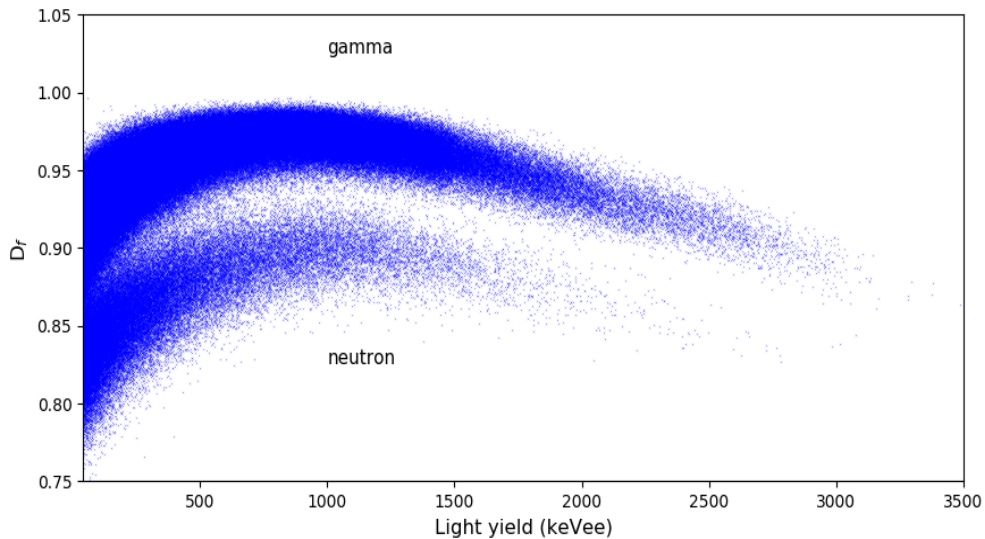


Figure 4: Scatter plot of PSD performed using CCM for the plastic scintillator sample exposed to the neutron/gamma-ray field of ^{252}Cf . There were 908,037 samples accepted in the process. Lower discrimination level was set to 40 keVee.

The experiment was performed by placing the ^{137}Cs radioactive source in the green holder. The top surface of the lead supporting plate was covered with a 2.5×2.5 mm grid, which was used to aid the movement of the coded aperture across the supporting plate. Each location of the 169 cell tungsten aperture was examined by moving the aperture across the grid, where each location was exposed to the radioactive source for 5 minutes, before moving on to the next cell.

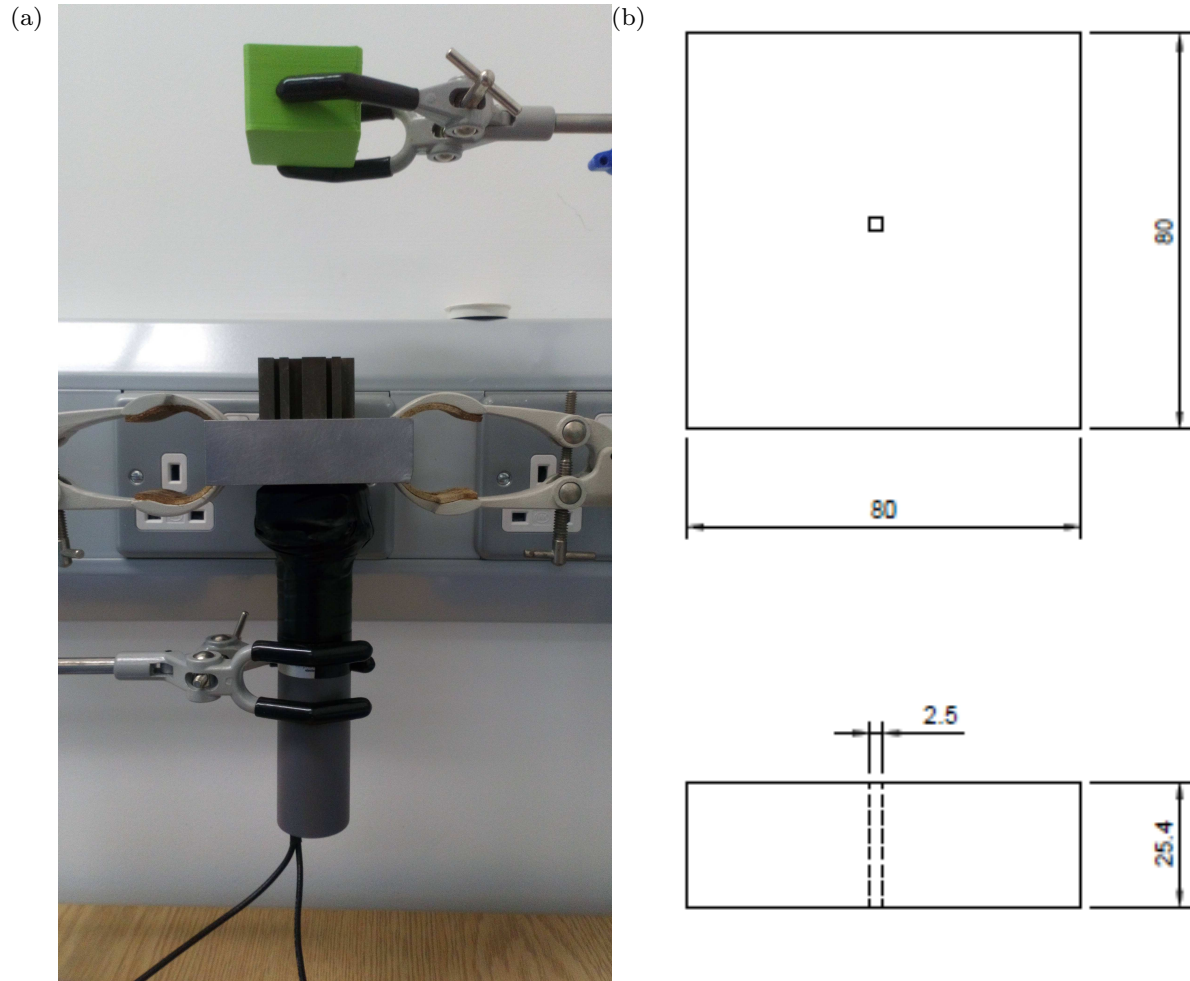


Figure 5: Equipment used in the experiment showing a) the entire experimental set-up comprising PMT and scintillator assembly, supporting lead plate, tungsten coded aperture, and source holder, and b) perspective CAD drawing of the supporting plate, with dimensions specified (mm).

3 Results

Before the first measurements of the ^{137}Cs modulated gamma-ray field were taken, the complete experimental set-up was tested without the coded aperture on top of the lead plate. This was used as an example to verify the energy spectrum obtained after 5 min exposure. Fig. 6 shows that the ^{137}Cs Compton edge can be clearly identified. In this 5 minute exposure window, 9315 pulses were detected. When completed, the aperture was placed back on top of the supporting plate and the measurement of the first location of the coded aperture was taken. The detector set-up was exposed for 5 minutes in this location, before the aperture was in turn moved to each of the remaining 168 locations. Background checks were performed daily throughout the duration of the experiment. These were executed by collecting data within the 5 minutes acquisition window, with no source in place and contributed on average, to approximately 1%.

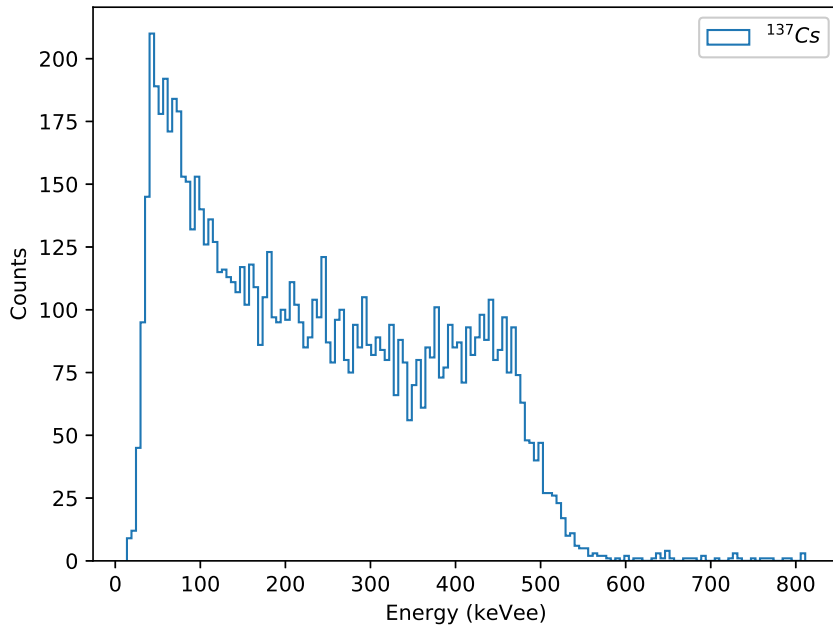


Figure 6: Pulse height spectra of ^{137}Cs , obtained by exposing of the source in the experimental set-up, but without the coded aperture in place. Measurements were taken over a 5 min exposure window.

3.1 Modulation properties of tungsten coded aperture

The collected data were arranged into a two dimensional array. Overall, 613,998 pulses were accepted through the pile-up rejection algorithm. The lowest count was around 1500 pulses, and the highest count over 9000 pulses. The lowest count corresponds to the area of the aperture where the cell under investigation is surrounded by opaque cells. The highest count was recorded in a clear area in the corner of the aperture where the transparent cell is also surrounded by transparent cells. The modulation image of the data is shown in Fig. 7.

It can be noticed that the modulation image in Fig. 7 does not fully correspond to the aperture design presented in Fig. 1. Opaque and transparent elements of the aperture are very difficult to distinguish and the overall pattern is equally difficult to recognise. However, some trends can be noticed. The areas of the image with the highest number of counts, i.e. approximately between 7000 and 9000 counts, are accumulated around the area where the single open aperture cells are not bounded by closed cells.

Counts between approximately 4000 and 6000 are associated with the areas of the aperture where there are only single cell or larger opening areas, for instance the area very close to the centre of the image, but these areas are surrounded by closed spaces. This indicates that the modulation provided by the closed areas of the coded aperture affects the neighbouring open spaces, as a result of gamma-ray interactions with the tungsten aperture blocks. Finally, the lowest count numbers (<4000) can be linked to the closed areas of the aperture. Hence, despite the fact that a quick visual inspection does not seem to resemble the design, closer examination does allow us to recognise useful patterns, including parts of the main body of the aperture.

3.2 Coded aperture image reconstruction

According to the rules of designing a coded aperture based on MURAs, an image detected by the sensitive detector is encoded through the aperture pattern. Therefore, the reconstruction process takes longer, when compared to other imaging methods, such as single pinhole collimator based detectors. However, the advantage is that the resolution of the reconstructed image is higher. The method responsible for encoding the image in MURA based apertures is convolution. Consequently, the decoding of the image

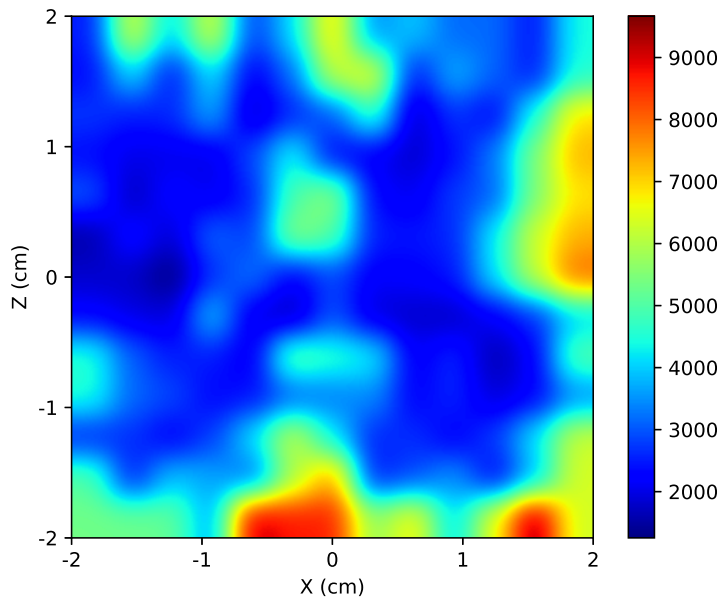


Figure 7: Image obtained based on the data received when the coded aperture was exposed to ^{137}Cs and in turn moved across the supporting plate to access its modulation properties. Colourbar values correspond to number of counts.

is achieved by deconvolution methods. A response for such analysis is expected to approximate the delta function [6].

Localisation of the ^{137}Cs source has been performed using a customised square deconvolution script implemented in Python. Initial inspection of the reconstructed image in Fig. 8 clearly indicates that the source was recognised in the centre of the aperture. This result has been obtained despite the imperfect modulation provided by the aperture indicated by Fig. 7. However, there is a noticeable spread of the reconstructed source over three cells of the aperture located in the centre of the reconstructed image. This suggests that the response is not in a form of a perfect delta function, as there are three impulses normalised to unity. This result is also indicated by the colourbar in Fig. 8.

It should also be noted that the illustrative results presented above have been obtained using a very specific experimental set-up, which was primarily designed for the analysis of aperture modulation properties. An additional aim was to verify the operation of the decoding algorithm. Given the basic assumptions of the design and implementation of the coded aperture imaging systems based on MURAs, a nearly perfect response, following the decoding, can be expected. A response approximating a delta function can only be obtained, if nearly perfect encoding occurs. Also the source must be reconstructed through the specific algorithm, which accounts for the pattern of the aperture used. In this work, the encoding of the radioactive source was of acceptable quality. However, the arrangement was sufficient for the deconvolution algorithm to place the reconstructed image in the centre of the aperture, as required.

4 Discussion

The results presented in the previous section suggest that a pure tungsten coded aperture, with a small cell size $2.8 \times 2.8 \times 25 \text{ mm}^3$, provide sufficient modulation of the gamma-ray field to reconstruct the source location. It could be argued that the localisation is not ideal, even though the the aperture was tested cell by cell, enabling the highest gamma-ray yield to be produced for every investigated cell directly. However, the results show the source on the expected location, and the spread over the three cells lies within standard statistical error boundaries.

Given the set-up chosen for this particular study, there is a small chance of some gamma-ray photons

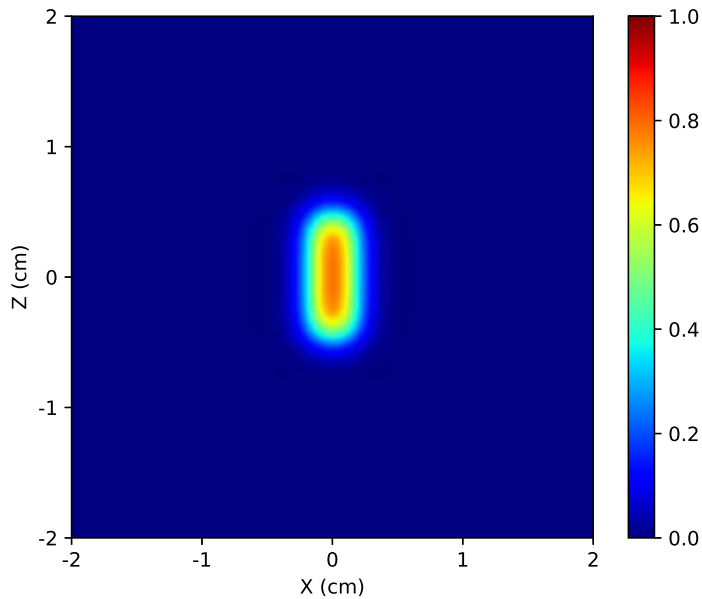


Figure 8: Reconstructed location of the source using deconvolution encoding. The image was obtained based on the data collected for each aperture location and arranged into a 13×13 array.

interacting with lead atoms in the supporting block. These can travel from the source, through any open area of the coded aperture, even those that are not investigated at a specific time. Hence, they could be accidentally detected by the scintillator detector. In a similar way, particles modulated through the aperture could still travel through the Pb block, and contribute to adding misclassified counts to specific cells. It is believed such interference caused the image in Fig. 7 to not fully represent the shape of the coded aperture.

Although the coded aperture examined in this study is eventually aimed for operation in mixed radiation fields, it was decided to initially examine the system in a single particle radiation field, as reported in this article. Since the ^{137}Cs radioactive isotope is widely used for detector calibration, it was used in this study to determine if the results of 5 min exposures of a single aperture cell were sufficient to reconstruct the expected gamma-ray spectrum. If this was not achieved, the experiment for the specific cell was repeated.

4.1 Comparison of simulation and experimental studies

The experimental study presented in this paper shares a number of similarities with previously published simulation work [10]. However, there exist significant differences between the two studies that make the comparison troublesome. Further, this experimental study was designed to identify potential issues that may be encountered in real-life scenario.

The aim of the aforementioned simulation study was to identify the most suitable candidate for the aperture material out of three chosen $\text{W-}^{113}\text{Cd}$ compositions. The aperture used in the experimental work, on the other hand, was built purely using tungsten due to safety concerns related to the handling of ^{113}Cd . Therefore, it was decided to only assess the gamma-ray stopping properties of the tungsten aperture. It follows that only gamma-ray emitters were used to investigate the performance of the aperture.

It should also be noted that the simulation study was based on neutron/photon flux or energy deposited, as measured within a scintillator cell. In such scenario, the scintillator cell acts as a perfect detector, whereas the experiment relies on the number of neutrons/photons interacting in the scintillator. Moreover, this experimental study was primarily aimed at assessing the ability to moderate the gamma-ray field sufficiently to localise the source.

Given the experimental scenario used, it is also difficult to assess number of particles reaching the scintillator that got through the aperture in the neighbouring cells, as well as other transparent aperture elements located farther from the cell under examination. As the supporting plate was designed to attenuate the gamma-ray spectrum in the neighbouring cells, it proved to be sufficient given the correctly reconstructed image, despite the imperfect modulation provided by the tungsten coded aperture.

5 Conclusions

Based on the results and discussion presented, it can be deduced that the tungsten coded aperture investigated in this work provides a sufficient level of gamma-ray modulation. As such, it offers the possibility of incorporating the aperture into a portable mixed-field radiation imaging system, owing to the small size of the part. Moreover, in comparison with the part designed for simulation work (Fig. 1a), the manufactured tungsten aperture does not have a bracket around its main body (Fig. 1b). This change was dictated by the possibility of placing the aperture in an enclosure [10], which would allow for adjustment of the field of view (FOV) depending on the specific requirements of an application.

The plastic organic scintillator used in this study offers a very good neutron/gamma separation down to 40 keVee. This provides an opportunity to use the system as a single- or dual-particle detection device. The second particle type could be either ignored or included, and secondary imaging provided for the other particle type. It would also become possible to have more coded apertures manufactured using different materials, such as the aforementioned ^{113}Cd , to target other particle types, given the replaceable character of the aperture. Finally, it would also be advantageous to test the tungsten coded aperture in a mixed-field environment, to appraise if the neutron modulation level is sufficient.

In future work, it is also intended to replace the single block scintillation detector with a pixelated form of an organic plastic scintillator. Such a scintillator has already been manufactured and is currently being characterised [16]. Moreover, various photodetectors and the accompanying readout electronics options are being considered, ranging from the standard multi-anode photomultiplier tubes (PMTs) to pixelated Silicon Photomultipliers (SiPMs). As a general rule, the former option offers better noisy immunity, whereas the latter offers a small footprint and is easier to implement in the system, since it does not require high voltage supply to operate. Both options have been extensively compared with regard to time resolution and PSD capabilities [17, 18].

Acknowledgements

The authors would like to acknowledge the funding support from EPSRC (EP/M507891/1 and EP/R02572X/1), the Faculty of Science and Technology (Lancaster University, UK) and Sellafield Ltd. The authors would like to express their gratitude to Dr. Natalia Zaitseva and the team at LLNL for providing the plastic scintillator sample. The authors also acknowledge the use of the Matplotlib package for all plots presented in this paper [19].

References

- [1] X. Li, A. Stevens, J. A. Greenberg, and M. E. Gehm, “Single-shot memory-effect video OPEN,” *Scientific Reports*, vol. 8, p. 13402, 2018.
- [2] A. Vella, A. A. Munoz, M. J. Healy, D. W. Lane, and D. Lockley, “An artificial X-ray wire test emitter and calculations on the resolution and field of view of X-ray pinhole optics by simulation,” *Nuclear Instruments and Methods in Physics Research, Section A: Accelerators, Spectrometers, Detectors and Associated Equipment*, vol. 905, pp. 119–128, 2018.
- [3] T. Lee, S. W. Kwak, and W. Lee, “Investigation of nuclear material using a compact modified uniformly redundant array gamma camera,” *Nuclear Engineering and Technology*, vol. 50, no. 6, pp. 923–928, 2018.
- [4] C. V. Griffith, R. S. Woolf, and B. F. Philips, “64-Element Fast-Neutron, Coded-Aperture Imager,” *IEEE International Symposium on Technologies for Homeland Security (HST)*, pp. 1–5, Apr. 2017.

- [5] C. Lynde, F. Carrel, V. Schoepff, C. Frangville, R. Woo, A. Sardet, J. Venara, M. B. Mosbah, R. A. Khalil, and Z. El Bitar, “Demonstration of coded-aperture fast-neutron imaging based on Timepix detector,” *Nuclear Inst. and Methods in Physics Research, A*, Article In Press, Available online Oct. 2018.
- [6] M. J. Cieślak, K. A. A. Gamage, and R. Glover, “Coded-aperture imaging systems: Past, present and future development – A review,” *Radiation Measurements*, vol. 92, pp. 59–71, 2016.
- [7] R. H. Dicke, “Scatter-Hole Cameras for X-Rays and Gamma Rays,” *The Astrophysical Journal*, vol. 153, p. L101, Aug. 1968.
- [8] E. E. Fenimore and T. M. Cannon, “Coded aperture imaging with uniformly redundant arrays,” *Applied Optics*, vol. 17, no. 3, pp. 337-347, 1978.
- [9] J. Newby, P. Hausladen, M. Blackston, and J. F. Liang, “Performance of Fast-Neutron Imaging Detectors Based on Plastic Scintillator,” *ORNL/TM-2013/82, Oak Ridge National Laboratory*, 2013.
- [10] M. J. Cieślak, K. A. A. Gamage, and R. Glover, “Investigation into a suitable scintillator and coded-aperture material for a mixed-field radiation imaging system,” *Journal of Instrumentation*, vol. 12, pp. P12007–P12007, Dec. 2017.
- [11] S. R. Gottesman and E. E. Fenimore, “New family of binary arrays for coded aperture imaging.,” *Applied optics*, vol. 28, no. 20, pp. 4344–4352, 1989.
- [12] M. J. Cieślak, K. A. A. Gamage, and R. Glover, “Pulse shape discrimination characteristics of stilbene crystal, pure and ^6Li loaded plastic scintillators for a high resolution coded-aperture neutron imager,” *Journal of Instrumentation*, vol. 12, no. 7, Jul. 2017.
- [13] F. Brooks, “A scintillation counter with neutron and gamma-ray discriminators,” *Nuclear Instruments and Methods*, vol. 4, pp. 151–163, Apr. 1959.
- [14] G. F. Knoll, *Radiation Detection and Measurement*, 4th Edition, John Wiley & Sons, Hoboken, 2010.
- [15] N. Zaitseva, A. Glenn, H. P. Martinez, L. Carman, I. Pawelczak, M. Faust, S. Payne, Pulse shape discrimination with lithium-containing organic scintillators, *Nuclear Instruments and Methods in Physics Research Section A: Accelerators, Spectrometers, Detectors and Associated Equipment* 729 (2013) 747–754. doi:10.1016/j.nima.2013.08.048.
- [16] M. J. Cieślak and K. A. A. Gamage, “Localised response retrieval from Hamamatsu H9500 for a coded aperture neutron-gamma imaging system based on an organic pixelated plastic scintillator (EJ-299-34),” *21st IEEE Real Time Conference*, pp. 8–10, 2018.
- [17] T. Szczesniak, M. Moszynski, M. Grodzicka, D. Wolski, Swiderski, M. Szawlowski, and M. Kapusta, “Time resolution of scintillation detectors based on SiPM in comparison to photomultipliers,” *IEEE Nuclear Science Symposium Conference Record*, pp. 1728–1735, 2010.
- [18] M. L. Ruch, C. B. Sivels, S. A. Czyz, M. Flaska, and S. A. Pozzi, “Comparison between silicon photomultipliers and photomultiplier tubes for pulse shape discrimination with stilbene,” *2014 IEEE Nuclear Science Symposium and Medical Imaging Conference, NSS/MIC 2014*, pp. 2–4, 2016.
- [19] J. D. Hunter, “Matplotlib: A 2d graphics environment,” *Computing in Science & Engineering*, vol. 9, pp. 90–95, 05 2007.